Journal of Materials Chemistry C

ROYAL SOCIETY OF CHEMISTRY

PAPER

View Article Online
View Journal | View Issue

Cite this: J. Mater. Chem. C, 2025, 13, 18724

The effect of critical micelle concentration on the amphiphilic species response using P3HT-based organic electrochemical transistors

Tatiana Gregorio,[a] Iris Miraballes,[bc] Dominique Mombrú,[*a] Mariano Romero[*a] and Alvaro W. Mombrú[*a]

Received 30th May 2025,
Accepted 8th August 2025

DOI: 10.1039/d5tc02122g

rsc.li/materials-c

Here, we present a proof-of-concept approach to study the effect of critical micelle concentration on alkyl sulfonate amphiphilic species response using organic electrochemical transistors (OECT) working in the accumulation mode. First of all, the drastic enhancement of the OECT response allows us to estimate the critical micelle concentration of alkyl sulfonate amphiphilic species yielding quite similar values compared to bulk solution conductivity experiments reported in the literature. Above the critical micelle concentration (*i.e.* 100 mM), the best responsive OECT devices yielded ON/OFF ratios of 30–60, maximum normalized transconductance of $g^{*}_{max} = 1.99 - 1.39\ mS\ cm^{-1}$ and threshold voltage of $-V_{th}$ = 0.39–0.55 V at V_g = −1.0 V. Our impedance spectroscopy studies performed at ON and OFF modes suggested that, in the presence of a sufficiently strong negative gate voltage (V_g = −1.0 V), not only the sodium counterions are ejected from the interface, but also the amphiphilic molecules from the monolayer probably reverse their orientation and get injected into the P3HT region. In this scenario, the sulfonate groups of the amphiphilic species synchronously induce doping of P3HT thus leading to a drastic enhancement of the channel current above the critical micelle concentration. Our results indicate that OECT devices represent a promising platform to estimate the critical micelle concentration of amphiphilic species but also to study the formation of amphiphilic monolayers of more complex systems of biological interest.

1. Introduction

Organic electrochemical transistors (OECTs) are one of the most promising sensing devices that can operate in aqueous media and are particularly interesting for transducing and amplifying low-amplitude ionic fluctuations of biological interest.[1] The OECTs can operate in depletion (*i.e.* the positive biasing of the gate electrode introduces cations into the semiconducting polymer leading to a decrease in the channel current) or accumulation (*i.e.* the negative biasing of the gate electrode introduces anions into the semiconducting polymer leading to an increase in the channel current) mode. The corresponding most frequent materials used as a channel for each working mode are poly(3,4-ethylenedioxythiophene) doped with poly(styrenesulfonate) (PEDOT:PSS)[2–4] and the undoped poly(3-hexylthiophene) (P3HT) and all its glycolated side chain analogs,[5,6] respectively. Particularly, the use of P3HT without glycolated side chain modification as channel materials is usually reserved for electrolyte-gated organic field-effect transistors (EGOFET) rather than an OECT considering its hydrophobic nature.[7–12] However, although P3HT swelling abilities are limited compared to its glycolated side chain analogs, there are a lot of studies suggesting that charge transport and transfer processes are far from being only a simple interface phenomenon. Huang *et al.* have reported that they produce P3HT porous films with controlled morphologies without the aid of polymer additives, enhancing OECT properties for hydrophobic polymers with efficient doping, fast ion intercalation/de-intercalation, high transconductance and capacitance.[13] The performance of P3HT-based OECTs has been improved by the preparation of a nanofiber microstructure, not only offering a porous interface with electrolytes but also promoting efficient ionic penetration and doping of the conjugated polymers.[14] The ionic fluctuations of biological origin refer to basic physiological indicators such as body temperature, blood pressure, blood oxygen levels, and heart rate, but can also refer to clinically

[a] Centro NanoMat & Área Física, Departamento de Experimentación y Teoría de la Estructura de la Materia y sus Aplicaciones (DETEMA), Facultad de Química, Universidad de la República, Montevideo C.P. 11800, Uruguay. E-mail: dmombru@fq.edu.uy, mromero@fq.edu.uy, amombru@fq.edu.uy
[b] Inmunología Clínica (BIOCLIN), Facultad de Química, Universidad de la República, Montevideo C.P. 11800, Uruguay
[c] Laboratorio de Biotecnología (Instituto Polo Tecnológico de Pando), Facultad de Química, Universidad de la República, Canelones C.P. 91000, Uruguay

relevant disease-specific biomolecules such as nucleic acid fragments, proteins, and metabolic molecules.[15,16] The most studied analytes using OECT devices working in depletion or accumulation mode are typically hydrophilic, *e.g.* simple ionic species such as hydronium, sodium, potassium, fluoride, chloride and bromide,[17,18] metabolites such as lactic acid,[19–21] ascorbic acid,[22] sialic acid,[23–25] uric acid,[26–28] hormones such as epinephrine,[29–31] neurotransmitters such as dopamine and acetylcholine[32–34] and more complex systems such as deoxyribonucleic acid and proteins.[35–38] However, other metabolites of biological interest with hydrophobic nature have been much less explored. For instance, an OECT-based electrochemical sensor for the selective detection of vitamin A in the form of retinyl acetate has been reported recently but using an organic electrolytic solution.[39] In between, there are other metabolites with an amphiphilic nature such as surfactants but also the particular case of fatty acids and their corresponding salts that are extremely relevant in different biological processes have not been studied yet. An amphiphilic compound is a term used to describe a compound containing a large organic cation or anion that possesses a long unbranched hydrocarbon chain. The existence of distinct polar (hydrophilic) and nonpolar (hydrophobic) regions in the molecule promotes the formation of micelles in aqueous solution.[40] In addition, it is well known that the amphiphilic species form these micelles above a certain concentration [*i.e.* the critical micelle concentration (c.m.c.)] while the amphiphilic species are more or less isolated in the diluted regime. The c.m.c. determination of amphiphilic species in bulk solutions has been typically studied by conductivity, surface tension, fluorescence and dynamic light scattering measurements.[41] Furthermore, the formation of micelles above the critical micelle concentration is accompanied by the formation of monolayers at both air and electrode interfaces. In the case of solid–liquid interfaces, not only monolayers and bilayers but a wide variety of surface micelles on solid surfaces have been found, such as hemicylinders, cylinders, hemispheres, and spheres.[42] Here, typical experimental methodologies include direct observation using atomic force microscopy (AFM) but also electrophoretic light scattering (ELS), which offers a rapid, high-resolution technique for the study of a wide variety of samples but not so straightforward for small micelles of surfactants whose sizes are in the range of only a few nanometers.[42] The use of self-assembled lipid bilayers on PEDOT:PSS-based electrodes and transistors as promising platforms for biosensing purposes has been reported recently,[43–45] but in the case of P3HT-based transistors, only chemically bonded lipid monolayers have been studied.[46,47] However, the later cases only use the amphiphilic species as biocompatible platforms to sense different metabolites but, to the best of our knowledge, there have been no approaches to studying the interaction and detection of amphiphilic species with P3HT using organic electrochemical transistors. Here, we present a proof-of-concept approach to study the effect of critical micelle concentration on the amphiphilic species response using a P3HT-based OECT working in the accumulation mode.

2. Methodology

2.1. Preparation of OECT devices

The OECT devices with coplanar geometry were prepared using thin gold gate, source and drain electrodes which were sputtered onto a glass substrate in a 0.2 mbar argon atmosphere at 30 mA DC sputtering ion current for 300 s using a removable insulating polymeric template (Scotch® Magic™ Tape 810HK) defining a channel area with length $L \sim 20$ μm and widths $W \sim 1000$ μm. Then, 5 μL of P3HT (SIGMA-ALDRICH CAS 104934-50-1: regioregular >90%, average M_w 50 000–75 000) dissolved in toluene with 10 mg ml^{-1} concentration was deposited on the channel area and dried at 100 °C for 60 minutes, yielding a thickness $d \sim 2$ μm. It is important to note that the OECT channel thickness is relatively high compared to typical values reported in the literature (*e.g.* 0.1 to 1.4 μm).[48–50] However, as we have no prior information about amphiphilic species interaction with P3HT-based OECTs, the use of thicker films can be justified by favoring the expected enhancement of transconductance at the expense of response times declining, as already observed in the literature for both hydrophobic and hydrophilic cases.[48–50] The same insulating polymeric mask was then deposited, leaving only the channel and gate area exposed to different amphiphilic electrolyte solutions based on the sodium alkyl sulfonates $C_nH_{2n+1}SO_3Na$ (n = 4, 6, 8, 10 and 12) with concentrations ranging from 1 to 100 mM, as schematized in Fig. S1. In addition, sodium lauryl sulfate ($C_{12}H_{25}SO_4Na$) was also studied to evaluate the role of amphiphilic head groups and sodium chloride (NaCl) was studied to evaluate the role of ionic strength. All the electrolyte salts were provided by SIGMA-ALDRICH and used without prior purification.

2.2. Characterization of OECT devices

The P3HT films comprising the OECT devices were characterized using grazing incidence small- and wide-angle X-ray scattering and microRaman imaging, as detailed and depicted in Fig. S2 and S3, respectively. The hydrodynamic diameter and zeta potential of the amphiphilic electrolytes were determined using the particle size/zeta potential analyzer Nano-ZS (Malvern Instruments Ltd) in an aqueous medium at 25 and 30 °C, for n = 10 and 12, respectively.

The hydrodynamic diameter was evaluated using dynamic light scattering (DLS) and reported as the z-average, while zeta potential was calculated from the electrophoretic mobility using the Helmholtz–Smoluchowski equation. The contact angle measurements were performed using the Sessile Drop Method. Each sample was analyzed in triplicate. X-ray reflectometry (XRR) was performed using Rigaku Ultima IV diffractometer with Cu Kα radiation working in parallel beam configuration. XRR patterns were used to estimate the critical angle and rugosity of P3HT films exposed to electrolytes below and above the critical micelle concentration. The channel current (I_{ds}) for our OECT devices was collected between the source and drain electrodes in the V_{ds} = −1.0 V to 0.0 V drain–source voltage range and different applied gate voltages between the gate and the source electrodes in the V_g = −1.0 V to 0.0 V range using the Keithley 2450 source-meter. In each case, the gate voltages were applied for several minutes to assure equilibrium conditions before each measurement, and

then each output data point was collected for 240 seconds until current stabilization. Impedance spectroscopy data were also collected between the gate and short-circuited source–drain electrodes of the OECT devices using Gamry Reference 3000 galvanostat/potentiostat working with an AC voltage amplitude of $V_{g,ac}$ = 20 mV in the 0.1 Hz–100 kHz frequency range at the OFF ($V_{g,dc}$ = 0.0 V) and ON ($V_{g,dc}$ = −1.0 V) modes. All electrical characterizations were performed inside an isolated Faraday cage at 25 °C and 50% RH ambient conditions.

3. Results and discussion

First of all, it is important to mention that the solubility of $C_nH_{2n+1}SO_3Na$ (n = 4, 6, 8 and 10) aqueous electrolytes was observed below 100 mM concentrations for all amphiphilic species at 25 °C. The c.m.c. reported for $C_nH_{2n+1}SO_3Na$ (n = 4, 6, 8, 10 and 12) aqueous solutions at room temperature is c.m.c. ∼8–10 mM for n = 12, ∼43–45 mM for n = 10, and above 100 mM for n < 10, according to the literature,[41] as schematized in Fig. 1(a). Our dynamic light scattering experiments corroborate the formation of micelles with a corresponding hydrodynamic mean size between ∼2.1–3.0 nm, and the zeta potential exhibited a crossover at ∼5–8 mM for n = 12 and at ∼40–50 mM for n = 10, in good agreement with the bulk solution c.m.c. values, as depicted in Fig. 1(b). It is important to mention that the larger size region was omitted for clarity and that both the hydrodynamic mean size and zeta potential are quite expected in comparison with those reported in the literature.[51] X-ray reflectometry (XRR) profiles of P3HT films

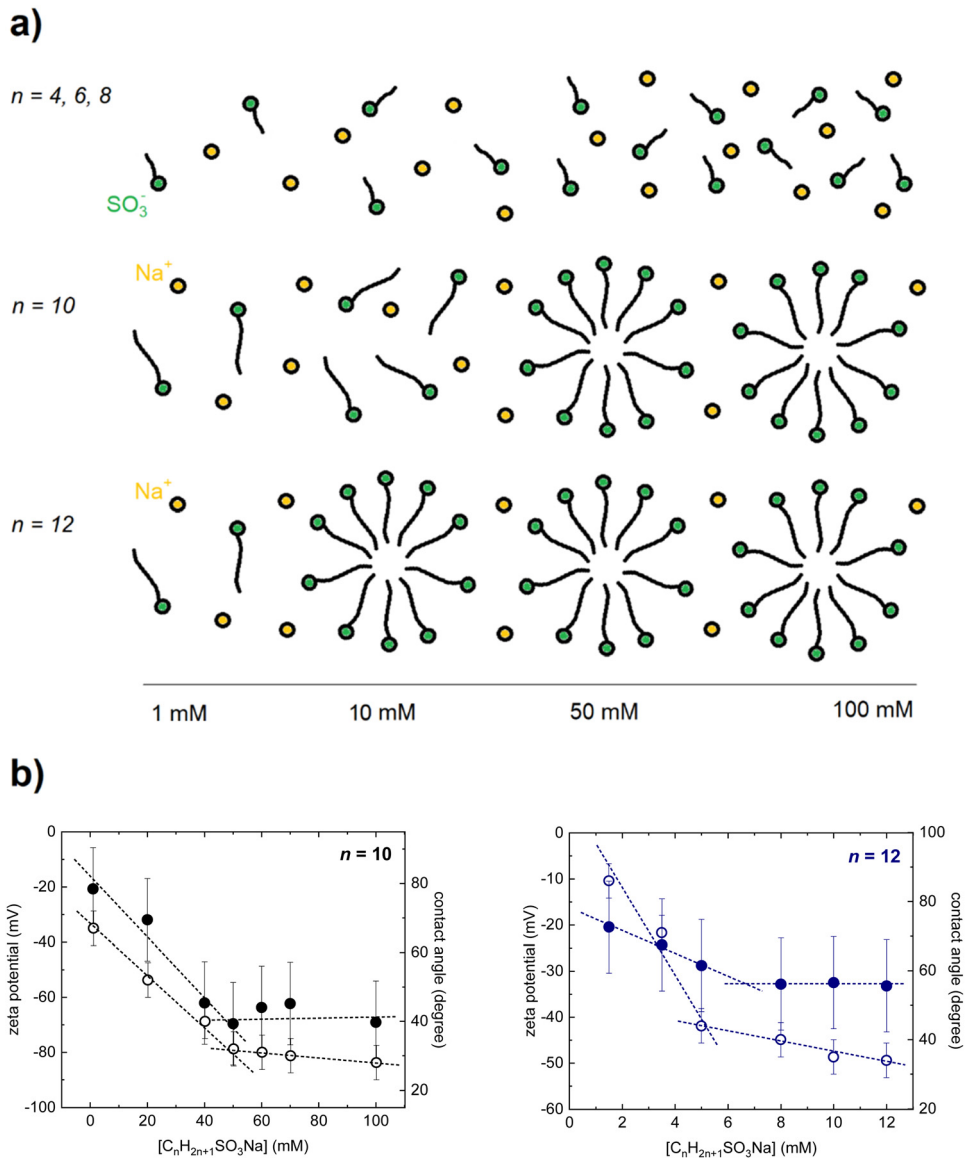

Fig. 1 (a) Schematization of critical micelle concentration for $C_nH_{2n+1}SO_3Na$ (n = 4, 6, 8, 10 and 12) and (b) zeta potential (full circles) and contact angle (hollow circles) at different $C_nH_{2n+1}SO_3Na$ concentrations for n = 10 and 12, at 25 and 30 °C, respectively.

exposed at different $C_nH_{2n+1}SO_3Na$ concentrations for n = 10 and 12, at 25 and 30 °C, respectively, are depicted in the upper panel of Fig. 2. The critical angle observed at $\theta_c \sim 0.46^\circ$ is mostly associated with the silicate glass substrate and the critical angle of P3HT film is probably masked at lower angles, as already observed for similar cases in the literature.[52] However, the smoothness of the XRR profile indicates that the film thickness is not thin enough, *i.e.* ~2 μm according to our Raman imaging analysis displayed in Fig. S3, to define the typical Kiessing fringes oscillation patterns observed for thinner films.[53]

In order to have more fine detail of X-ray reflectometry analysis, the $I(q)\cdot q^4$ *vs.* q plots are plotted and analyzed. The presence of broad oscillations that are frequently associated with ultrathin layers (*i.e.* <3 nm) is observed for all cases and a clear shift toward lower q values is progressively observed with increasing amphiphilic species concentration until almost stabilized at ~40 mM (for n = 10) and at ~5 mM (for n = 12), in good agreement with bulk solution c.m.c. values. Although the data does not allow the confirmation of the formation of a well-defined monolayer, the formation of a stabilized ultrathin layer comprised of amphiphilic species above the P3HT film is in good agreement with the formation of micelles observed for bulk solution experiments discussed earlier. The contact angle images for P3HT films exposed at different $C_nH_{2n+1}SO_3Na$ concentrations for n = 10 and 12, at 25 and 30 °C, respectively, are shown in the lower panel of Fig. 2. The contact angles showed a marked decrease from ~67° at 1 mM until stabilized on ~30° at ~40 mM (for n = 10) and showed a marked decrease from ~86° at 1 mM until stabilized on ~40° at ~5 mM (for n = 12), as depicted in Fig. 1(b), in agreement with the formation of micelles observed for bulk solution experiments discussed earlier.

The output characteristics collected at fixed V_{ds} = −0.8 V and V_g = −1.0 V for P3HT-based OECT working with $[C_nH_{2n+1}SO_3Na]$ with n = 4, 6, 8, 10 and 12 at different electrolyte concentrations ranging between 1–100 mM at 25 °C are displayed in the left panel of Fig. 3. It is quite interesting to note that, while n < 10 species exhibit a soft increase in $-I_{ds}$ with increasing concentration, n = 10 exhibits a sudden notorious increase in $-I_{ds}$ just above the c.m.c. (*i.e.* ~50 mM).

In the case of n = 12, we also observed a sudden but less marked increase just below its corresponding c.m.c., *i.e.* ~4–6 mM. However, it is important to mention that this value is shifted to

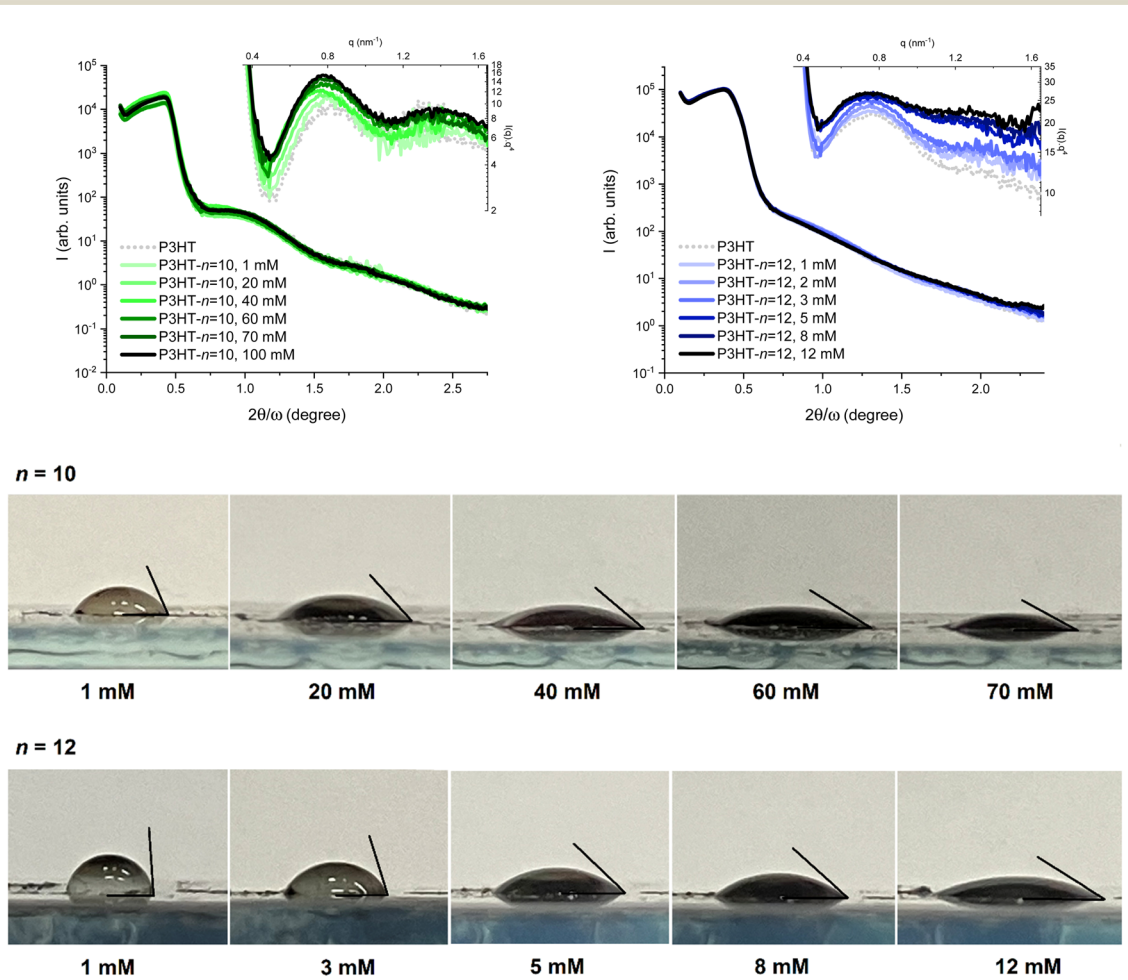

Fig. 2 X-ray reflectometry (XRR) curves depicted as $I(q)$ *vs.* $2\theta/\omega$ and $I(q)\cdot q^4$ *vs.* q plots (upper panel) and contact angle images (lower panel) for P3HT films exposed at different $C_nH_{2n+1}SO_3Na$ concentrations for n = 10 and 12, at 25 and 30 °C, respectively.

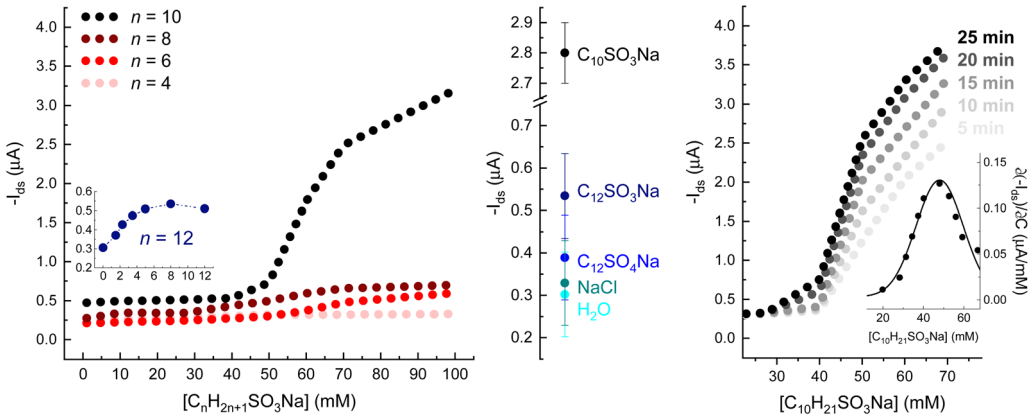

Fig. 3 Output data collected at fixed V_{ds} = −0.8 V and V_g = −1.0 V for P3HT-based OECT working with $C_nH_{2n+1}SO_3Na$ with n = 4, 6, 8, 10 and 12 at different electrolyte concentrations ranging between 1–100 mM at 25 °C (left panel), working with $C_{12}H_{25}SO_3Na$ and $C_{12}H_{25}SO_4Na$ just above their c.m.c. (*i.e.* ∼8–10 mM), NaCl at 10 mM and distilled water at 25 °C (middle panel) and working with n = 10 at different stabilization times and the corresponding first derivative for stabilized data at 25 °C (right panel).

lower values compared to literature (*i.e.* ∼8–10 mM)[41] as similarly observed for n = 12 when interacting with polymers in solution.[51] Interestingly, *n*-alkyl sulfonates with shorter alkyl chains, such as n = 10, do not exhibit drastic shifting of c.m.c. when interacting with polymers in solution.[51] In addition, it is also important to note that the OECT response for n = 12 exhibited considerably lower channel current values above c.m.c. compared to those observed for n = 10. This suggests that the amphiphilic species c.m.c. value strongly affects the OECT response and, particularly, those with higher c.m.c. values exhibited a more marked response. In addition, we also plot the $-I_{ds}$ values obtained at fixed V_{ds} = −0.8 V and V_g = −1.0 V for sodium lauryl sulfonate ($C_{12}H_{25}SO_3Na$) and sulfate ($C_{12}H_{25}SO_4Na$) near above their c.m.c. (*i.e.* ∼8–10 mM) to evaluate the role of different amphiphilic head groups, as shown in the middle panel of Fig. 3. It is observed that the electrolyte response is higher for sodium lauryl sulfonate ($C_{12}H_{25}SO_3Na$) compared to sodium lauryl sulfate ($C_{12}H_{25}SO_3Na$). This difference can be related to the higher oxidant properties of sulfonate with respect to sulfate head groups, considering that both species present the same alkyl chain and very similar c.m.c. values. However, it is important to note that their $-I_{ds}$ values are slightly higher compared to NaCl 10 mM aqueous solution, indicating that the doping abilities of amphiphilic species with lower c.m.c. values (such as n = 12 alkyl sulfonates) are comparable to the effect of ionic strength and, thus, are much poorer than those with higher c.m.c. values (such as n = 10 alkyl sulfonates). The right panel of Fig. 3 shows the output characteristic data collected for n = 10 electrolyte in the same conditions as mentioned earlier at different stabilization times, indicating that the OECT reaches stable values after 25 minutes. These relatively long stabilization times probably refer to the slow formation kinetics of the amphiphilic species monolayer on the polymeric surface, but also to the slow ionic diffusion kinetics when injected into the conducting polymer. Furthermore, this is relevant to obtain more accurate values for the critical micelle concentration by using the first derivative maximum, yielding c.m.c. = (48.0 ± 1.8) mM. Similarly, but not shown in the figure, the c.m.c. for n = 12 electrolyte estimated using the same procedure yielded c.m.c. = (3.6 ± 0.7) mM. Here, we are demonstrating that our c.m.c. estimation using a P3HT-based OECT device yielded quite similar values compared to bulk solution conductivity experiments reported in the literature.[41]

It is noteworthy to mention that in these cases, we are obtaining information not only about the micelle but also about the monolayer formed at the interface with the conductive polymer. We expanded the characterization of OECT devices working with the more sensitive electrolyte above the c.m.c. to evaluate the micelle and monolayer effect on the OECT response. Thus, the corresponding output, transfer and hysteresis transfer characteristics for P3HT-based OECT working with n = 10 electrolyte at 25 °C above its c.m.c. value; *i.e.* 0.1 M, are shown in Fig. 4. The output and transfer characteristics, as well as the transconductance and threshold voltage plots for P3HT-based OECT working with n = 12 electrolyte at 30 °C just above its c.m.c. value; *i.e.* 8 mM, are shown in Fig. S4. It is important to note that the output characteristic showed a deviation from the typical saturation behavior, as already observed to be especially prevalent in hydrophobic materials with alkyl side chains.[54–56] This deviation can probably be associated with a spatially non-uniform hole mobility throughout the volume of the channel with regard to the transistor pinch-off operating in a mixed OECT/EGOFET regime.[17] In fact, for n = 10, the transistor output characteristic switches from a linear regime at V_{ds} ∼ −0.2 V but only reaches a quasi-saturation regime at V_{ds} ∼ −0.8 V, which could be considered an underestimation of the pinch-off voltage, as depicted in Fig. 4(a). For n = 10 above c.m.c., the transfer characteristics exhibited $-I_{ds,V_g=-1.0V}$ values ranging from 7.26, 6.12, 5.24 and 4.20 μA and ON/OFF ratios (estimated using the $-I_{ds,V_g=-1.0V}/-I_{ds,V_g=0.0V}$ ratio) ranging from 32, 39, 47 and 60 for V_{ds} = −1.0, −0.8, −0.6 and −0.4 V, respectively. The transfer hysteresis curve of the OECT devices evidenced a notorious difference between forward and

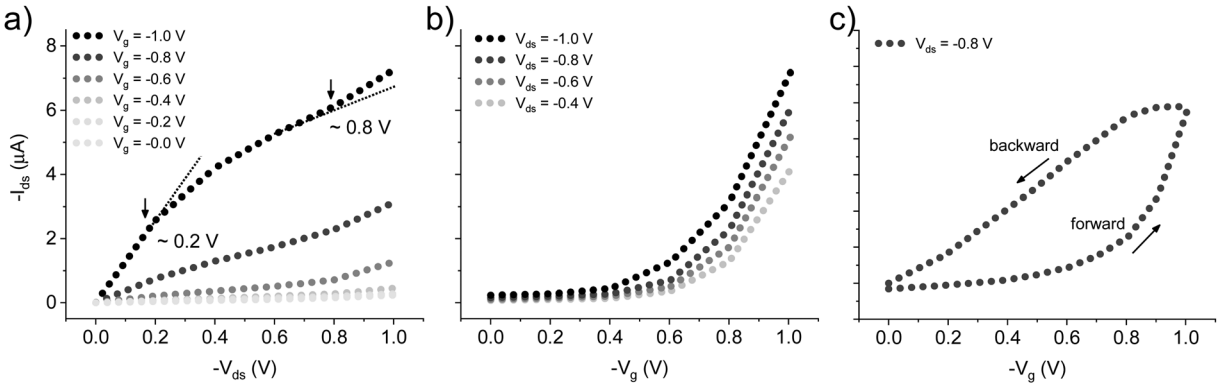

Fig. 4 (a) Output ($-I_{ds}$ *vs.* $-V_{ds}$ at selected V_g values), (b) transfer ($-I_{ds}$ *vs.* $-V_g$ at selected V_{ds} values) and (c) hysteresis transfer ($-I_{ds}$ *vs.* $-V_g$ at selected V_{ds} value in forward and backward directions) characteristics for P3HT-based OECT working with [$C_{10}H_{21}SO_3Na$] 0.1 M electrolyte at 25 °C. The voltages at which the transistor output characteristic switches from linear to quasi-saturation regime are marked with arrows.

backward transfer characteristics. Typically, P3HT-based OECT devices exhibited a capacitive hysteresis behavior described by the higher absolute values of the current in the backward direction with respect to the forward direction.[57] However, the great difference between forward and backward transfer characteristics is expected for such a large anion with limiting ionic transport.[57] It is important to note that the transfer hysteresis curve was collected using a slow scan rate ($\sim$0.5 mV s^{-1}) to minimize the contribution to the hysteresis behavior due to fast scan rates. The hysteresis behavior can thus be attributed mostly to the slow ionic injection/ejection dynamics and the limitations of ion diffusion kinetics.[57] The transconductance (g_m) defined as $g_m = |\partial I_{ds}/\partial V_g|$ and the square root current ($|I_{ds}|^{1/2}$) as a function of V_g at fixed $V_{ds} = -0.8$ V are plotted in Fig. 5. The maximum normalized transconductance ($g^*_{max} = g_{max}L/Wd$) exhibited $g^*_{max} = 1.99,\ 1.85,\ 1.68$ and 1.39 mS cm^{-1} values, while the threshold voltage (V_{th}) obtained from the *x*-axis interception exhibited $-V_{th}$ = 0.39, 0.46, 0.52, and 0.55 V values for V_{ds} = −1.0, −0.8, −0.6 and −0.4 V, respectively. For n = 12 above c.m.c., the output and transfer characteristics exhibited about ten times lower $-I_{ds}$ values compared with n = 10 above c.m.c., as also observed in the $-I_{ds}$ *vs.* concentration plots depicted in the left panel of Fig. 3.

For instance, n = 12 above c.m.c. exhibited $-I_{ds,V_g=-1.0V}$ values ranging from 0.55, 0.44 and 0.35 μA and ON/OFF ratios (estimated using the $-I_{ds,V_g=-1.0V}/-I_{ds,V_g=0.0V}$ ratio) ranging from 1.3, 1.4, 1.5 for V_{ds} = −1.0, −0.8 and −0.6 V, respectively, as depicted in Fig. S4. To provide insights into the ionic transport, injection and ionic–electronic charge transfer properties of these P3HT-based OECT devices, we performed impedance spectroscopy studies. The total impedance (Z) response can be defined as a function of the real part (Z') and the imaginary part (Z'') of impedance, as follows:

$$Z = Z' - iZ''$$

The Nyquist plots ($-Z''$ *vs.* Z') and the Bode plots (ϕ *vs.* f and $|Z|$ *vs.* f) at the OFF ($V_{g,dc}$ = 0.0 V) and ON ($V_{g,dc}$ = −1.0 V) modes for n = 10 and 12 are depicted in Fig. 6 and Fig. S5, respectively. The volumetric capacitance (C^*) can be estimated from the plateau observed at low frequencies for the total capacitance response but, in our case, the presence of a small deviation at low frequencies indicates a non-ideal behavior which is more appropriate to study using a circuit model fitting.[58] Our impedance data showed best fitting with a circuit model based on a resistor (R_{ion}) (representing the electrolyte transport in

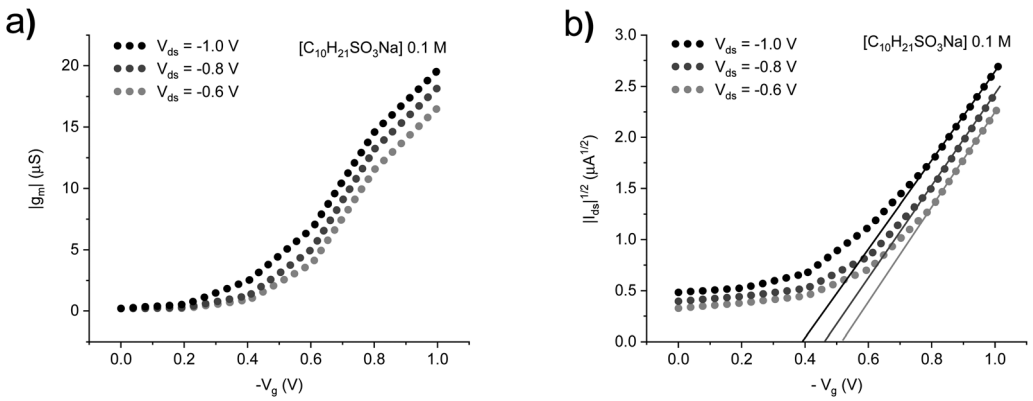

Fig. 5 (a) Transconductance (g_m *vs.* V_g at selected V_{ds} values) and (b) threshold voltage ($|I_{ds}|^{1/2}$ *vs.* V_g at selected V_{ds} values) plots for P3HT-based OECT working with [$C_{10}H_{21}SO_3Na$] 0.1 M electrolyte at 25 °C.

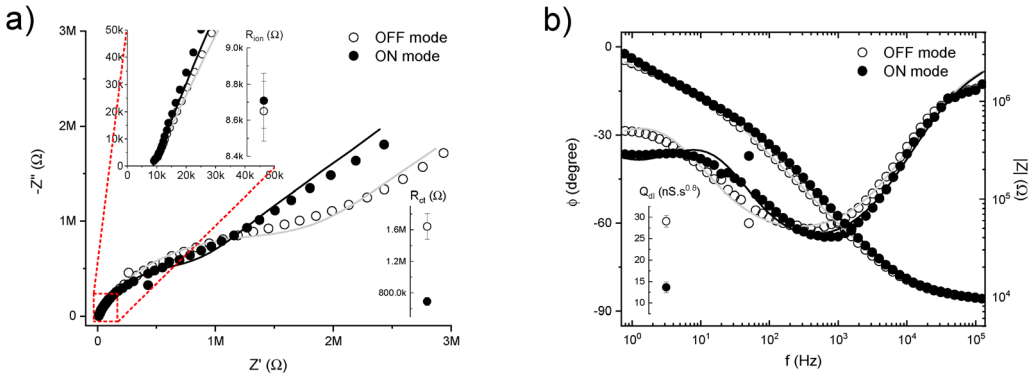

Fig. 6 (a) Nyquist and (b) Bode plots for P3HT-based OECT working with [$C_{10}H_{21}SO_3Na$] 0.1 M electrolyte at 25 °C for different operation modes; *i.e.* OFF ($V_{g,dc}$ = 0.0 V) and ON ($V_{g,dc}$ = −1.0 V).

solution) connected in series with the parallel combination of resistor – diffusive-like constant phase element and capacitive-like constant phase element (R_{ct}//CPE) (representing the electrolyte diffusion and charge transfer processes), as depicted in Fig. S6. The constant phase element (CPE) impedance can be described by the following equation:

$$Z_{CPE} = (1/Q)/(i\omega)^{\alpha}$$

where Q (admittance at ω = 1 rad s^{-1}) and α (exponent) are frequency-independent parameters, with α = 1 and 0 representing an ideal capacitor and resistor, respectively, while α = 0.5 is associated with diffusion processes.[59] The fitted bulk solution ionic resistance (R_{ion}) values were 8.83 ± 0.15/8.74 ± 0.15 kΩ (n = 10) and 32.51 ± 0.54/37.16 ± 0.61 kΩ (n = 12) for ON/OFF modes, respectively. The similarity between both values is quite expected considering that the micelles are at the same concentration. On the other hand, the fitted charge transfer resistance (R_{ct}) values were 803 ± 68/1579 ± 211 kΩ (n = 10) and 426 ± 166/578 ± 117 kΩ (n = 12) and the non-ideal capacitor constant phase element (Q_{CPE}) values were 15.1 ± 1.2/28.5 ± 1.3 nS s^{α} (n = 10) and 59.2 ± 6.4/130 ± 14 nS s^{α} (n = 12) with $\alpha \sim 0.8$ for ON/OFF modes, respectively.

The decrease in the charge transfer resistance and pseudo-capacitance clearly indicates that the negative gate voltage induces interesting molecular rearrangements at the interface. These results allow us to consider some scenarios to understand the charge transfer processes at the interface between the amphiphilic electrolyte monolayer and the conductive polymer comprising the OECT channel. A possible scenario implies that, in the absence of any gate voltage, the amphiphilic electrolyte monolayer is formed at the interface with the sulfonate heads exposed to the aqueous medium and the hydrophobic alkyl chains interacting with the hydrophobic P3HT polymer. Then, in the presence of a sufficiently strong negative gate voltage (*e.g.* V_g = −1.0 V), not only the sodium counterions ejected from the interface, but also the amphiphilic molecules from the monolayer probably synchronously reverse their orientation and get injected into the P3HT region, as depicted in Fig. 7. This scenario implies that the monolayer can be reversed completely or partially, but this synchronous reversion enhances the interaction of sulfonate groups with thiophene rings, inducing

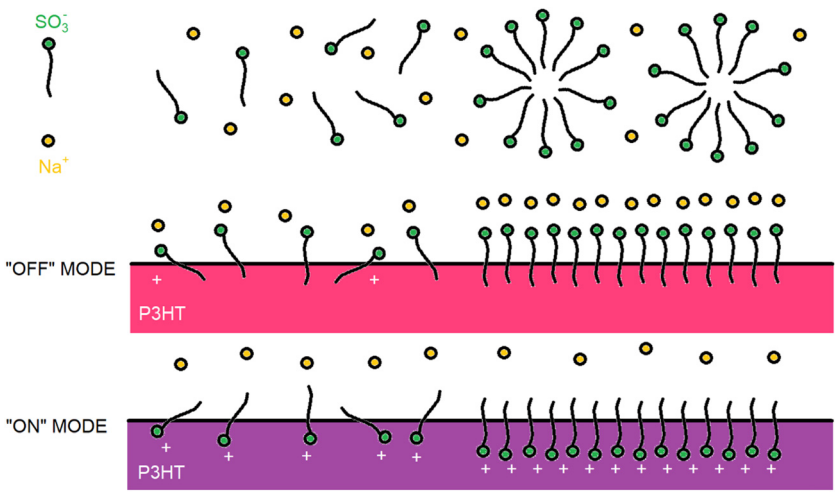

Fig. 7 Schematization of the formation of a monolayer in the electrolyte/P3HT interface above the critical micelle concentration and its effect on the "OFF" and "ON" states for P3HT-based OECT.

the doping of P3HT and thus the enhancement in the channel current, as is well understood in the literature.[60] It is noteworthy to note that the response of amphiphilic species with lower c.m.c. values (such as n = 12 alkyl sulfonates) are much poorer than those with higher c.m.c. values (such as n = 10 alkyl sulfonates).

This could be related to the formation of more condensed monolayers compared to the more expanded monolayers formed by amphiphilic species with higher and lower c.m.c. values, respectively.[61] Below the critical micelle concentration, there is only a diluted and isolated interaction of the amphiphilic species sulfonate groups with P3HT and thus the OECT response enhancement is expected to be less pronounced. This can be associated with the surface adsorption of sulfonate ions near the P3HT interface, even in the absence of severe penetration into the bulk film, which could produce electrostatic doping effects *via* local field modulation. In addition, the increase in ionic strength with increasing surfactant concentration may also enhance electrochemical coupling, screening effects, or double-layer capacitance at the interface, thus yielding less pronounced enhancement on the OECT response.

4. Conclusions

In the present report, we present a proof-of-concept approach to study the effect of critical micelle concentration on the amphiphilic species response using organic electrochemical transistors working in the accumulation mode. First of all, by using our OECT devices, we estimate the critical micelle concentration of alkyl sulfonate amphiphilic species, yielding quite similar values compared to bulk solution conductivity experiments reported in the literature. Above the critical micelle concentration, the OECT devices working with *n*-alkyl sulfonates (n = 12) yielded ON/OFF ratios of 30–60, maximum normalized transconductance of $g^*_{max} = 1.99 - 1.39$ mS cm^{-1} and threshold voltage of $-V_{th}$ = 0.39–0.55 V at V_g = −1.0 V. Our impedance spectroscopy studies performed at ON and OFF modes suggested that, in the presence of a sufficiently strong negative gate voltage (V_g = −1.0 V), not only the sodium counterions are ejected from the interface, but also the amphiphilic molecules from the monolayer probably synchronously reverse their orientation and get injected into the P3HT region. Our results indicate that OECT devices represent a promising platform to estimate the critical micelle concentration of amphiphilic species, but also to study the formation of amphiphilic monolayers of more complex systems of biological interest.

Author contributions

The manuscript was written through the contributions of all authors. All authors have given approval to the final version of the manuscript.

Conflicts of interest

There are no conflicts to declare.

Data availability

The data supporting this article have been included as part of the SI.

Schematization of the lateral and top view for the P3HT-based OECT devices working with different amphiphilic electrolyte solutions and an optical microscope image of the OECT channel showing its dimensions. Grazing incidence small-angle X-ray scattering and wide-angle X-ray scattering for P3HT films performed using Rigaku Ultima IV diffractometer with Cu Kα radiation working in parallel beam configuration. μRaman imaging and corresponding averaged Raman spectra for P3HT films performed using WITec alpha 300 RA with 532 nm laser wavelength and <10 mW laser power. The output and transfer characteristics, as well as the transconductance and threshold voltage plots for P3HT-based OECT working with [$C_{12}H_{25}SO_3Na$] 8 mM electrolyte at 30 °C. Nyquist and Bode plots for P3HT-based OECT working with [$C_{12}H_{25}SO_3Na$] 8 mM electrolyte at 30 °C for different operation modes; *i.e.* OFF ($V_{g,dc}$ = 0.0 V) and ON ($V_{g,dc}$ = −1.0 V). Equivalent circuit model used to fit the impedance spectroscopy data. See **https://doi.org/10.1039/d5tc02122g**

Acknowledgements

The authors thank the collaboration of Dr. Ricardo Faccio and Uruguayan Comisión Sectorial de Investigación Científica (CSIC), Agencia Nacional de Investigación e Innovación (ANII), and Programa de Desarrollo de las Ciencias Básicas (PEDECIBA) funding institutions. We particularly appreciate the financial support of ANII POS_NAC_2024_1_183297 PhD grant.

References

1 J. Rivnay, S. Inal, A. Salleo, R. M. Owens, M. Berggren and G. G. Malliaras, Organic electrochemical transistors, *Nat. Rev. Mater.*, 2018, **3**, 17086.
2 D. Khodagholy, J. Rivnay, M. Sessolo, M. Gurfinkel, P. Leleux, L. H. Jimison, E. Stavrinidou, T. Herve, S. Sanaur, R. M. Owens and G. G. Malliaras, High transconductance organic electrochemical transistors, *Nat. Commun.*, 2013, **4**, 2133.
3 L. Bießmann, L. P. Kreuzer, T. Widmann, N. Hohn, J. F. Moulin and P. Müller-Buschbaum, Monitoring the Swelling Behavior of PEDOT:PSS Electrodes under High Humidity Conditions, *ACS Appl. Mater. Interfaces*, 2018, **10**, 9865–9872.
4 M. Romero, D. Mombrú, F. Pignanelli, R. Faccio and A. W. Mombrú, Mixed Ionic-Electronic Transport for PEDOT:PSS-Based Zero-Gated Organic Electrochemical Transistors Using Impedance Spectroscopy and Micro-Raman Imaging, *ACS Appl. Electron. Mater.*, 2023, **5**(9), 4863–4874.
5 S. Inal, J. Rivnay, P. Leleux, M. Ferro, M. Ramuz, J. C. Brendel, M. M. Schmidt, M. Thelakkat and G. G. Malliaras, A High Transconductance Accumulation Mode Electrochemical Transistor, *Adv. Mater.*, 2014, **26**(44), 7450–7455.

6 J. Wagner, Y. Song, T. Lee and H. E. Katz, The combined influence of polythiophene side chains and electrolyte anions on organic electrochemical transistors, *Electrochem. Sci. Adv.*, 2022, **2**, 2100165.
7 E. Macchia, K. Manoli, B. Holzer, C. Di Franco, M. Ghittorelli, F. Torricelli, D. Alberga, G. F. Mangiatordi, G. Palazzo, G. Scamarcio and L. Torsi, *Nat. Commun.*, 2018, **9**, 3223.
8 P. Seshadri, K. Manoli, N. Schneiderhan-Marra, U. Anthes, P. Wierzchowiec, K. Bonrad, C. Di Franco and L. Torsi, *Biosens. Bioelectron.*, 2018, **104**, 113.
9 S. P. White, C. D. Frisbie and K. D. Dorfman, *ACS Sens.*, 2018, **3**, 395–402; E. Macchia, K. Manoli, B. Holzer, C. Di Franco, R. A. Picca, N. Cioffi, G. Scamarcio, G. Palazzo and L. Torsi, *Anal. Bioanal. Chem.*, 2019, **411**, 4899.
10 E. Macchia, L. Sarcina, R. A. Picca, K. Manoli, C. Di Franco, G. Scamarcio and L. Torsi, *Anal. Bioanal. Chem.*, 2020, **412**, 811.
11 L. Sarcina, F. Viola, F. Modena, R. A. Picca, P. Bollella, C. Di Franco, N. Cioffi, M. Caironi, R. Osterbacka, I. Esposito, G. Scamarcio, L. Torsi, F. Torricelli and E. Macchia, *Anal. Bioanal. Chem.*, 2022, **414**, 5657.
12 L. Sarcina, E. Macchia, G. Loconsole, G. D'Attoma, P. Bollella, M. Catacchio, F. Leonetti, C. Di Franco, V. Elicio, G. Scamarcio, G. Palazzo, D. Boscia, P. Saldarelli and L. Torsi, *Adv. Sci.*, 2022, **9**, 2203900.
13 L. Huang, Z. Wang, J. Chen, B. Wang, Y. Chen, W. Huang, L. Chi, T. J. Marks and A. Facchetti, Porous Semiconducting Polymers Enable High-Performance Electrochemical Transistors, *Adv. Mater.*, 2021, **33**, 2007041.
14 Y. H. Tung, C. Y. Li, Y. C. Huang and Y. C. Lin, Strategically Tailoring Porous Polythiophene Nanofibers in Organic Electrochemical Transistors To Facilitate the Anion Doping, *ACS Electrochem.*, 2025, **1**(7), 1164–1175.
15 J. Song, H. Liu, Z. Zhao, P. Lin and F. Yan, Flexible organic transistors for biosensing: devices and applications, *Adv. Mater.*, 2024, **36**(20), 2300034.
16 H. Liu, J. Song, Z. Zhao, S. Zhao, Z. Tian and F. Yan, Organic electrochemical transistors for biomarker detections, *Adv. Sci.*, 2024, **11**(27), 2305347.
17 L. Q. Flagg, R. Giridharagopal, J. Guo and D. S. Ginger, Anion-dependent doping and charge transport in organic electrochemical transistors, *Chem. Mater.*, 2018, **30**(15), 5380–5389.
18 L. Q. Flagg, C. G. Bischak, R. J. Quezada, J. W. Onorato, C. K. Luscombe and D. S. Ginger, P-type electrochemical doping can occur by cation expulsion in a high-performing polymer for organic electrochemical transistors, *ACS Mater. Lett.*, 2020, **2**(3), 254–260.
19 Y. Zhang, Y. Wang, X. Qing, Y. Wang, W. Zhong, W. Wang, Y. Chen, Q. Liu and D. Wang, Fiber organic electrochemical transistors based on multi-walled carbon nanotube and polypyrrole composites for noninvasive lactate sensing, *Anal. Bioanal. Chem.*, 2020, **412**, 7515–7524.
20 A. M. Pappa, D. Ohayon, A. Giovannitti, I. P. Maria, A. Savva, I. Uguz, J. Rivnay, I. McCulloch, R. Owens and S. Inal, Direct metabolite detection with an n-type accumulation mode organic electrochemical transistor, *Sci. Adv.*, 2018, **4**(6), eaat0911.
21 M. Braendlein, A. M. Pappa, M. Ferro, A. Lopresti, C. Acquaviva, E. Mamessier, G. Malliaras and R. M. Owens, Lactate detection in tumor cell cultures using organic transistor circuits, *Adv. Mater.*, 2017, **29**(13), 1605744.
22 L. Zhang, G. Wang, D. Wu, C. Xiong, L. Zheng, Y. Ding, H. Lu, G. Zhang and L. Qiu, Highly selective and sensitive sensor based on an organic electrochemical transistor for the detection of ascorbic acid, *Biosens. Bioelectron.*, 2018, **100**, 235–241.
23 R. Zhu, Y. Wang, Y. Tao, Y. Wang, Y. Chen, M. Li, Q. Liu, L. Yang and D. Wang, Layer-by-layer assembly of composite conductive fiber-based organic electrochemical transistor for highly sensitive detection of sialic acid, *Electrochim. Acta*, 2022, **425**, 140716.
24 L. Chen, N. Wang, J. Wu, F. Yan and H. Ju, Organic electrochemical transistor for sensing of sialic acid in serum samples, *Anal. Chim. Acta*, 2020, **1128**, 231–237.
25 X. Guo, J. Liu, F. Liu, F. She, Q. Zheng, H. Tang, M. Ma and S. Yao, Label-free and sensitive sialic acid biosensor based on organic electrochemical transistors, *Sens. Actuators, B*, 2017, **240**, 1075–1082.
26 A. Yang, Y. Li, C. Yang, Y. Fu, N. Wang, L. Li and F. Yan, Fabric organic electrochemical transistors for biosensors, *Adv. Mater.*, 2018, **30**(23), 1800051.
27 M. Galliani, C. Diacci, M. Berto, M. Sensi, V. Beni, M. Berggren, M. Borsari, D. Simon, F. Biscarini and C. A. Bortolotti, Flexible printed organic electrochemical transistors for the detection of uric acid in artificial wound exudate, *Adv. Mater. Interfaces*, 2020, **7**(23), 2001218.
28 Y. Tao, Y. Wang, R. Zhu, Y. Chen, X. Liu, M. Li, L. Yang, Y. Wang and D. Wang, Fiber based organic electrochemical transistor integrated with molecularly imprinted membrane for uric acid detection, *Talanta*, 2022, **238**, 123055.
29 N. Saraf, E. R. Woods, M. Peppler and S. Seal, Highly selective aptamer based organic electrochemical biosensor with pico-level detection, *Biosens. Bioelectron.*, 2018, **117**, 40–46.
30 N. Coppedè, G. Tarabella, M. Villani, D. Calestani, S. Iannotta and A. Zappettini, Human stress monitoring through an organic cotton-fiber biosensor, *J. Mater. Chem. B*, 2014, **2**(34), 5620–5626.
31 C. H. Mak, C. Liao, Y. Fu, M. Zhang, C. Y. Tang, Y. H. Tsang, H. L. W. Chan and F. Yan, Highly-sensitive epinephrine sensors based on organic electrochemical transistors with carbon nanomaterial modified gate electrodes, *J. Mater. Chem. C*, 2015, **3**(25), 6532–6538.
32 N. Wang, Y. Liu, Y. Fu and F. Yan, AC measurements using organic electrochemical transistors for accurate sensing, *ACS Appl. Mater. Interfaces*, 2018, **10**(31), 25834–25840.
33 X. Qing, Y. Wang, Y. Zhang, X. Ding, W. Zhong, D. Wang, W. Wang, Q. Liu, K. Liu, M. Li and Z. Lu, Wearable fiber-based organic electrochemical transistors as a platform for highly sensitive dopamine monitoring, *ACS Appl. Mater. Interfaces*, 2019, **11**(14), 13105–13113.
34 G. E. Fenoy, C. Von Bilderling, W. Knoll, O. Azzaroni and W. A. Marmisollé, PEDOT: Tosylate-Polyamine-Based

Organic Electrochemical Transistors for High-Performance Bioelectronics, *Adv. Electron. Mater.*, 2021, **7**(6), 2100059.
35 E. Macchia, K. Manoli, B. Holzer, C. Di Franco, M. Ghittorelli, F. Torricelli, D. Alberga, G. F. Mangiatordi, G. Pallazo, G. Scamarcio and L. Torsi, Single-molecule detection with a millimetre-sized transistor, *Nat. Commun.*, 2018, **9**(1), 3223.
36 P. Seshadri, K. Manoli, N. Schneiderhan-Marra, U. Anthes, P. Wierzchowiec, K. Bonrad, C. Di Franco and L. Torsi, Low-picomolar, label-free procalcitonin analytical detection with an electrolyte-gated organic field-effect transistor based electronic immunosensor, *Biosens. Bioelectron.*, 2018, **104**, 113–119.
37 J. Peng, T. He, Y. Sun, Y. Liu, Q. Cao, Q. Wang and H. Tang, An organic electrochemical transistor for determination of microRNA21 using gold nanoparticles and a capture DNA probe, *Microchim. Acta*, 2018, **185**, 1–8.
38 Y. Song, H. Zhang, T. Mukhopadhyaya, A. S. Hall and H. E. Katz, Sensitive organic electrochemical transistor biosensors: Comparing single and dual gate functionalization and different COOH-functionalized bioreceptor layers, *Biosens. Bioelectron.*, 2022, **216**, 114691.
39 L. Salvigni, F. Mariani, I. Gualandi, F. Decataldo, M. Tessarolo, D. Tonelli, B. Fraboni and E. Scavetta, Selective detection of liposoluble vitamins using an organic electrochemical transistor, *Sens. Actuators, B*, 2023, **393**, 134313.
40 P. Muller, Glossary of terms used in physical organic chemistry (IUPAC Recommendations 1994), *Pure Appl. Chem.*, 1994, **66**(5), 1077–1184.
41 P. Mukerjee and K. J. Mysels, Critical micelle concentrations of aqueous surfactant systems, NSRDS-NBS 36, National Bureau of Standards, 1971.
42 V. Paruchuri, A. V. Nguyen and J. D. Miller, Zeta-potentials of self-assembled surface micelles of ionic surfactants adsorbed at hydrophobic graphite surfaces, *Colloids Surf., A*, 2004, **250**, 519–526.
43 Z. Lu, D. van Niekerk, A. Savva, K. Kallitsis, Q. Thiburce, A. Salleo, A. M. Pappa and R. M. Owens, Understanding electrochemical properties of supported lipid bilayers interfaced with organic electronic devices, *J. Mater. Chem. C*, 2022, **10**(20), 8050–8060.
44 K. Bali, C. Guffick, R. McCoy, Z. Lu, C. F. Kaminski, I. Mela, R. Owens and H. W. van Veen, Biosensor for Multimodal Characterization of an Essential ABC Transporter for Next-Generation Antibiotic Research, *ACS Appl. Mater. Interfaces*, 2023, **15**(10), 12766–12776.
45 Z. Lu, C. Barberio, A. Fernandez-Villegas, A. Withers, A. Wheeler, K. Kallitsis, E. Martinelli, A. Savva, B. M. Hess, A. M. Pappa, G. S. Kaminski Schierle and R. M. Owens, Microelectrode Arrays Measure Blocking of Voltage-Gated Calcium Ion Channels on Supported Lipid Bilayers Derived from Primary Neurons, *Adv. Sci.*, 2024, **11**(27), 2304301.
46 T. P. Nguy, R. Hayakawa, V. Kilinc, M. Petit, S. N. Yemineni, M. Higuchi, J. M. Raimundo, A. M. Charrier and Y. Wakayama, Electrolyte-gated-organic field effect transistors functionalized by lipid monolayers with tunable pH sensitivity for sensor applications, *Appl. Phys. Express*, 2020, **13**(1), 011005.
47 T. P. Nguy, V. Kilinc, R. Hayakawa, C. Henry-De-Villeneuve, J. M. Raimundo, Y. Wakayama and A. Charrier, Affinity driven ion exchange EG-OFET sensor for high selectivity and low limit of detection of cesium in seawater, *Sens. Actuators, B*, 2022, **351**, 130956.
48 J. Rivnay, P. Leleux, M. Ferro, M. Sessolo, A. Williamson, D. A. Koutsouras, D. Khodagholy, M. Ramuz, X. Strakosas, R. M. Owens, C. Benar, J.-M. Badier, C. Bernard and G. G. Malliaras, High-performance transistors for bioelectronics through tuning of channel thickness, *Sci. Adv.*, 2015, **1**, e1400251.
49 A. G. Polyravas, N. Schaefer, V. F. Curto, A. Bonaccini Calia, A. Guimera-Brunet, J. A. Garrido and G. G. Malliaras., Effect of channel thickness on noise in organic electrochemical transistors, *Appl. Phys. Lett.*, 2020, **117**, 073302.
50 C. Yan, L. Xiang, Y. Xiao, X. Zhang, Z. Jiang, B. Zhang, C. Li, S. Di and F. Zhang., Lateral intercalation-assisted ionic transport towards high-performance organic electrochemical transistor, *Nat. Commun.*, 2024, **1**(5), 10118.
51 P. Yan and J. X. Xiao, Polymer–surfactant interaction: differences between alkyl sulfate and alkyl sulfonate, *Colloids Surf., A*, 2004, **244**(1–3), 39–44.
52 O. Werzer and R. Resel, Model-independent X-ray reflectivity fitting for structure analysis of poly(3-hexylthiophene) films, *Macromolecules*, 2013, **46**(9), 3529–3533.
53 M. Yasaka, X-ray thin-film measurement techniques, *Rigaku J.*, 2010, **26**(2), 1–9.
54 A.-M. Pappa, D. Ohayon, A. Giovannitti, I. Maria, A. Savva, I. Uguz, J. Rivnay, I. McCulloch, R. Owens and S. Inal, Direct Metabolite Detection with an N-Type Accumulation Mode Organic Electrochemical Transistor, *Sci. Adv.*, 2018, **4**, eaat0911.
55 A. Giovannitti, D.-T. Sbircea, S. Inal, C. B. Nielsen, E. Bandiello, D. A. Hanifi, M. Sessolo, G. G. Malliaras, I. McCulloch and J. Rivnay, Controlling the Mode of Operation of Organic Transistors through Side-Chain Engineering, *Proc. Natl. Acad. Sci. U. S. A.*, 2016, **113**, 12017–12022.
56 A. Giovannitti, K. J. Thorley, C. B. Nielsen, J. Li, M. J. Donahue, G. G. Malliaras, J. Rivnay and I. McCulloch, Redox-Stability of Alkoxy-BDT Copolymers and Their Use for Organic Bioelectronic Devices, *Adv. Funct. Mater.*, 2018, **28**, 1706325.
57 J. Bisquert, B. Ilyassov and N. Tessler, Switching Response in Organic Electrochemical Transistors by Ionic Diffusion and Electronic Transport, *Adv. Sci.*, 2024, **11**, 2404182.
58 D. Ohayon, V. Druet and S. Inal, A guide for the characterization of organic electrochemical transistors and channel materials, *Chem. Soc. Rev.*, 2023, **52**(3), 1001–1023.
59 M. E. Orazem and B. Tribollet, Electrochemical Impedance Spectroscopy, *Diffusion Impedance*, New Jersey, 2008, ch. 11, pp. 183–210.
60 D. Mombrú, M. Romero, R. Faccio and A. W. Mombrú, Unraveling the lithium bis (trifluoromethanesulfonyl) imide (LiTFSI) doping mechanism of regioregular poly(3-hexylthiophene): experimental and theoretical study, *J. Phys. Chem. C*, 2020, **124**(13), 7061–7070.
61 L. Peltonen, J. Hirvonen and J. Yliruusi, The Effect of Temperature on Sorbitan Surfactant Monolayers, *J. Colloid Interface Sci.*, 2001, **239**(1), 134–138.